A numerical study of natural convection in concentric and eccentric horizontal cylindrical annuli with mixed boundary conditions

C. J. Ho, Y. H. Lin, and T. C. Chen
Department of Mechanical Engineering, National Cheng Kung University, Tainan, Taiwan 70101, Republic of China

Received 15 October 1987 and accepted for publication 15 June 1988

Numerical solutions are presented for steady laminar two-dimensional natural convection in concentric and eccentric horizontal cylindrical annuli with constant heat flux on the inner wall and a specified isothermal temperature on the outer wall. The heat and fluid flow patterns in the annuli are vividly visualized by means of the contour maps of streamlines and heatlines. Results of the parametric study conducted further reveal that the influence of the Prandtl number is quite weak; the heat and fluid flows are primarily dependent on the modified Rayleigh number and the eccentricity of the annulus. Above all, the specification of different thermal boundary conditions has a significant effect on the average heat transfer rate across the annulus.

Keywords: natural convection; annuli; numerical solutions

Introduction

The problem of natural convection heat transfer across a horizontal cylindrical annulus has received considerable attention in view of its fundamental importance germane to numerous engineering applications. As a result, extensive experimental and theoretical works dealing with the flow and associated heat transfer characteristics of natural convection in such configuration have been reported in the literature. Comprehensive reviews on natural convection in concentric and eccentric annuli are available,[1–4] and there is no need to repeat them. However, most of the previous studies are concerned with the horizontal annulus enclosed by two isothermal cylinders; little attention has been paid to annuli with other types of thermal boundary conditions of engineering interest. Van de Sande and Hamer[5] have obtained empirical correlations for natural convection heat transfer in concentric and eccentric annuli of constant heat flux. Recently, Glakpe *et al.*[4] presented a numerical solution for air in concentric and eccentric configurations with specified constant heat flux at the boundaries.

To further extend the existing knowledge on natural convection heat transfer in horizontal cylindrical annulus, the consideration in the present study is given to laminar steady natural convection in concentric and eccentric horizontal cylindrical annuli with mixed boundary conditions. Specifically, the outer cylinder of the annulus is maintained isothermal at T_o while the inner cylinder is subjected to a uniform constant heat flux q_i. Numerical solutions of the physical configuration described above have been obtained by solving the governing partial differential equations. After the present study was completed, two numerical works on the similar problem were recently reported.[6,7] Kumar[6] considered natural convection of air in a concentric horizontal annulus of various diameter ratio between 1.2 to 10 with mixed boundary conditions. Glakpe and Watkins[7] addressed the effect of mixed boundary conditions on the natural convection in an air-filled concentric and eccentric annulus of diameter ratio fixed at 2.2; however, only a downward vertical eccentricity of 0.5 was considered for the eccentric geometry. It follows that despite the similarity between the physical configuration under consideration, there are differences in the medium nature and the geometric configuration between these two earlier studies and the present work. Still, comparisons were attempted, if possible, between the present computations and the results available in Refs. 6 and 7. In the present work, the effects of the mixed thermal boundary conditions on the heat and fluid flow across the annulus are vividly visualized by means of the contour maps of streamlines and heatlines. Heat transfer results of extensive parametric studies are presented also.

Formulation and numerical method

The geometric configuration under study here is a concentric or vertically eccentric arrangement of two horizontal circular cylinders of radii r_i and r_o. The downward eccentricity of the inner cylinder is denoted as positive e. The outer cylinder is cooled at a fixed temperature T_o while the inner cylinder is heated with a constant heat flux q_i. It is assumed that the flow in the annulus is laminar, steady, and two-dimensional. All fluid properties, except the density in the buoyancy force term, are taken to be constants. Also, it is assumed that the flow is symmetric about a vertical plane through the axis of the cylinder. Accordingly, attention is confined to the half-annulus only.

To deal with the numerical difficulty associated with the complex physical domain of the eccentric annulus, a radial coordinate transformation[8] is adopted to map the eccentric annular gap into a unit circle. The radial coordinate transformation is achieved by defining a new radial coordinate as

$$\eta=(r-R_i)/(F(\phi^+)-R_i) \tag{1}$$

where $F(\phi^+)$ denotes the dimensionless radial profile of the outer cylinder measured from the center of the inner cylinder and is given as

$$F(\phi^+)=[R_0^2-\varepsilon^2\sin^2(\phi^+)]^{1/2}-\varepsilon\cos(\phi^+) \tag{2}$$

The dimensionless equations governing the steady fluid motion in the horizontal annulus, using the Oberbeck-Boussinesq approximation and neglecting viscous dissipation

and compressibility effects, are then given in vorticity–stream function formulation as follows:

$$\frac{1}{\pi r}\frac{\partial \eta}{\partial r}\left(\frac{\partial \psi}{\partial \phi}\frac{\partial \omega}{\partial \eta}-\frac{\partial \psi}{\partial \eta}\frac{\partial \omega}{\partial \phi}\right)=\Pr \hat{\nabla}^2\omega+\Pr \mathrm{Ra}^* \cdot\left[\sin(\pi\phi)\frac{\partial \eta}{\partial r}\frac{\partial \theta}{\partial \eta}+\frac{\cos(\pi\phi)}{\pi r}\left(\frac{\partial \theta}{\partial \phi}+\frac{\partial \eta}{\partial \phi}\frac{\partial \theta}{\partial \eta}\right)\right] \tag{3}$$

$$\hat{\nabla}^2\psi=-\omega \tag{4}$$

$$\frac{1}{\pi r}\frac{\partial \eta}{\partial r}\left(\frac{\partial \psi}{\partial \phi}\frac{\partial \theta}{\partial \eta}-\frac{\partial \psi}{\partial \eta}\frac{\partial \theta}{\partial \phi}\right)=\hat{\nabla}^2\theta \tag{5}$$

where

$$\frac{\partial \eta}{\partial r}=\frac{1}{F-R_i} \tag{6a}$$

$$\frac{\partial \eta}{\partial \phi}=\frac{-\eta}{F-R_i}\frac{\partial F}{\partial \phi} \tag{6b}$$

$$\frac{\partial^2 \eta}{\partial \phi^2}=\frac{-1}{F-R_i}\left(\eta\frac{\partial^2 F}{\partial \phi^2}+2\frac{\partial \eta}{\partial \phi}\frac{\partial F}{\partial \phi}\right) \tag{6c}$$

$$\hat{\nabla}^2\equiv\left[\left(\frac{\partial \eta}{\partial r}\right)^2-\left(\frac{1}{\pi r}\frac{\partial \eta}{\partial \phi}\right)\right]\frac{\partial^2}{\partial \eta^2}+\frac{2}{(\pi r)^2}\frac{\partial \eta}{\partial \phi}\frac{\partial^2}{\partial \eta\,\partial \phi}+\frac{1}{(\pi r)^2}\frac{\partial^2}{\partial \phi^2}+\left[\frac{1}{r}\frac{\partial \eta}{\partial r}+\frac{1}{(\pi r)^2}\frac{\partial^2 \eta}{\partial \phi^2}\right]\frac{\partial}{\partial \eta} \tag{6d}$$

The associated boundary conditions for the problem considered are

$$\phi=0 \text{ or } 1: \quad \frac{\partial \theta}{\partial \phi}=\psi=\omega=0 \tag{7a}$$

$$\eta=0: \quad \frac{\partial \theta}{\partial \eta}=R_i-F, \qquad \psi=\frac{\partial \omega}{\partial \eta}=0 \tag{7b}$$

$$\eta=1: \quad \theta=0, \quad \psi=\frac{\partial \psi}{\partial \eta}=0 \tag{7c}$$

From the above formulation, the governing parameters for the present problem are thus the modified Rayleigh number Ra*, the Prandtl number Pr, the radius ratio r_o/r_i, and the eccentricity ε.

Equations 3–7 are solved by a finite difference method. Finite difference equations were derived by using central difference approximations for the partial derivatives except the convective terms for which a quadratic upwind difference formula was employed.[9] At grids adjacent to the solid boundaries where the quadratic upwind differencing scheme was not applied, the second upwind scheme was used. The finite difference analogue of the governing equations along with the boundary conditions was then solved by iteration. The equations of temperature and vorticity were solved by successive line relaxation method,[10] while the stream function equation was solved by the modified strongly implicit (MSI) procedure.[11] The solution was considered convergent when the relative error between the new and old values of the field variables (ω, ψ, and θ) becomes less than a prescribed criterion (10^{-5}). Further, the convergence of the steady-state solution was verified by checking the balance between the overall heat transfer rate at the inner and outer cylinder within 1%. A nonuniform grid field has been used for the radial direction, which has a smoothly varying grid spacing with a denser grid near both the inner and outer walls of the annulus to account for the boundary layers formed in these regions. Based on several trial cases, suitable grid systems were selected for the present calculations. Two different grid systems depending on the geometry have been used for the calculations: 45 (radial direction) by 41 (angular direction) for $\varepsilon=0$ and 51 by 45 for $\varepsilon=\pm 0.625$. The computations were performed on an IBM 4381 computer and required less than 1200 CPU seconds for a typical case.

Results and discussion

Numerical calculations have been performed systematically for an annulus of radius ratio fixed at 2.6 to investigate the parametric influences on the heat and fluid flow patterns and

Notation

e	Vertical eccentricity
F^+	Radial profile of outer cylinder
F	Dimensionless radial profile of outer cylinder, F^+/L
g	Gravitational acceleration
h	Heat transfer coefficient
H	Dimensionless heat function, Equation 8
k	Thermal conductivity
L	Annular gap, r_0-r_i
Nu	Nusselt number, hL/k
Pr	Prandtl number
q	Heat flux
r^+	Radial coordinate
r	Dimensionless coordinate, r^+/L
Ra	Rayleigh number, $g\beta L^3\Delta T/\nu\alpha$
Ra*	Modified Rayleigh number, $g\beta q_i L^4/k\nu\alpha$
r_i	Radius of inner cylinder
R_i	Dimensionless radius of inner cylinder, r_i/L
r_o	Radius of outer cylinder
R_o	Dimensionless radius of outer cylinder, r_o/L
T	Temperature
ΔT	Average temperature difference between cylinders
V^+	Velocity
V	Dimensionless velocity, V^+L/α

Greek symbols

α	Thermal diffusivity
β	Thermal expansion coefficient
ε	Dimensionless vertical eccentricity e/L
η	Radial coordinate in transformed plane
θ	Dimensionless temperature, $(T-T_o)k/q_iL$
ν	Kinematic viscosity
ρ	Density
ϕ^+	Angular coordinate
ϕ	Dimensionless angular coordinate, ϕ^+/π
ψ^+	Stream function
ψ	Dimensionless stream function, ψ^+/α
ω^+	Vorticity
ω	Dimensionless vorticity, ω^+L^2/α

Subscripts

i, o	Inner and outer
r	Radial direction
ϕ	Angular direction

Superscript

$\bar{}$	Circumferentially averaged quantity

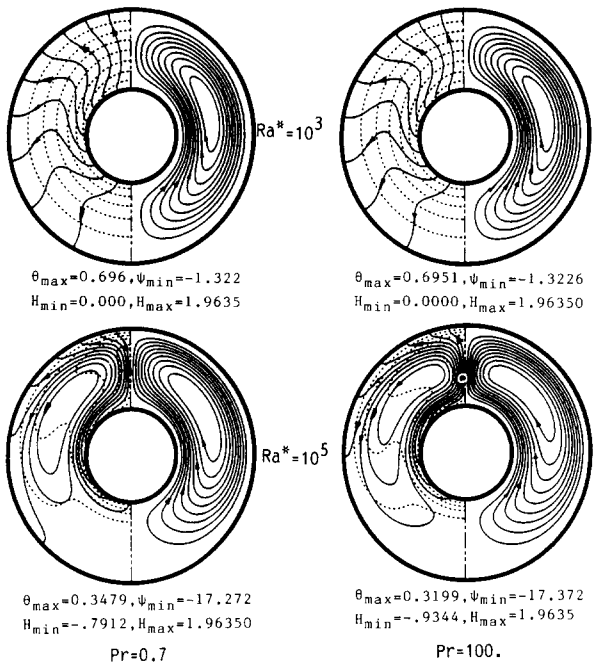

Figure 1 Influence of the modified Rayleigh number on heat and fluid flows. Streamlines (right) and heatlines (left) and isotherms (dashed lines)

heat transfer rate of the problem considered in the present study. The ranges of governing parameters covered in the calculations are $0.7 \leqq Pr \leqq 100$, $10^3 \leqq Ra^* \leqq 10^6$, and $\varepsilon = 0, \pm 0.625$.

Heat and fluid flows

In order to provide vivid visualization of convective heat flow pattern within the horizontal annulus, the concept of heat function introduced by Kiura and Bejan[12] is adopted in the present study. Here a dimensionless heat function H is defined as

$$\frac{1}{r}\frac{\partial H}{\partial \phi} = V_r\theta - \frac{\partial \theta}{\partial r} \tag{8a}$$

$$-\frac{\partial H}{\partial r} = V_\phi\theta - \frac{1}{r}\frac{\partial \theta}{\partial \phi} \tag{8b}$$

The computed heat and fluid flows will be presented qualitatively by means of streamlines, heatlines, and isotherm contour plots. The streamlines are plotted on the right half of the annulus, while the heatlines (solid lines) and isotherms (dashed lines) are drawn on the left half.

Figure 1 shows the effect of the modified Rayleigh number on the heat and fluid flow patterns in the concentric annulus for $Pr = 0.7$ and 100. At low Ra^* (10^3) the fluid flow in the half-annulus is weak and forms a symmetrical recirculation in the clockwise direction. With specified heat flux condition on the inner cylinder, some isotherms, as expected, originate from the inner wall of the annulus. The isotherms are nearly circular, further indicating little influence of the convective flow on heat transfer. Examination of the heatline distribution also reveals that heat leaving the inner cylinder is channeled rather directly to the outer cylinder as expected for the pseudoconduction heat transfer regime. Moreover, it appears that the Prandtl number has no apparent effect on the heat and fluid flow patterns at such a low value of Ra^*. As Ra^* increases, the fluid motion becomes stronger, as indicated by the increased absolute value of the stream function and the vortex center of the eddy shifts upward. At $Ra^* = 10^5$, the isotherm patterns exhibit features somewhat similar to those of the convection-dominated regime for isothermal boundary conditions available in the literature. A rather isothermal region at the bottom of the annulus can be readily observed. Furthermore, the heatline distribution in the figure indicates that heat from the inner cylinder is via thermal plume activity funneled through the top region above the inner cylinder, as evidenced by the clustered heatlines in the region, and then redistributed toward the outer cylinder, resulting in a core region with closed loops of heatlines that cannot release its enthalpy to the outer cylinder. Moreover, Figure 1 reveals that with increasing Ra^*, the heat-receiving region along the outer cylinder, where the heatlines end, becomes gradually smaller and tends to be restricted in the upper portion. That is, at high Ra^* heat from the inner wall is mainly transported to the upper half of the outer cylinder. The large gradient in the heatlines adjacent to the heated cylinder is due primarily to the rapid fluid motion. This signifies a convection-dominated heat flow across the annulus. Also, the recirculating heat flow pattern in the core region resembles that of recirculating fluid flow in the annulus.

Figure 2 presents the influence of the Prandtl number on the heat and fluid flows within the concentric annulus at $Ra^* = 10^6$. As the Prandtl number is increased from 0.7 to 7.0, the vortex center of recirculating flow moves closer to the symmetry line, and the isotherm and heatline distributions are significantly changed. With further increase of Pr, it can be readily seen from the figure that, for $Pr \geqq 7.0$, the variation of the Prandtl number produces no apparent effect on the heat and fluid flow patterns. Such finding about the effect of Pr on heat and fluid flow in the concentric annulus is similar to that reported for isothermal boundaries.[13,14]

Next, the heat and fluid flow patterns for the eccentric configurations considered in this study will be examined. Figures 3 and 4 illustrate the streamline, isotherm, and heatline distri-

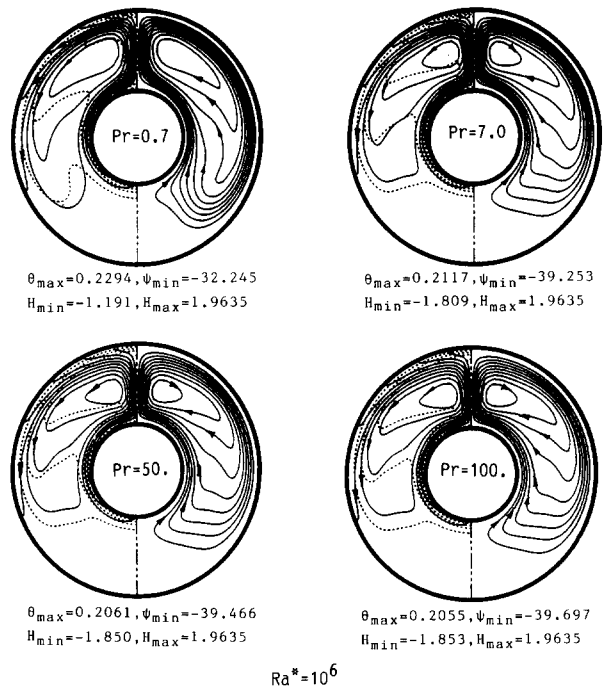

Figure 2 Effect of the Prandtl number on heat and fluid flows for concentric annuli at $Ra^* = 10^6$

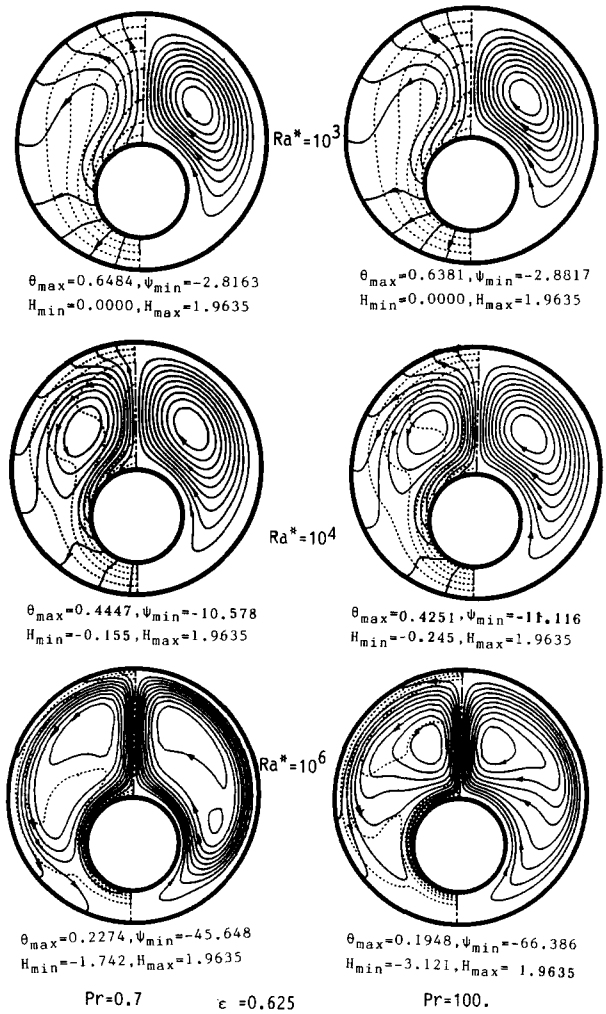

Figure 3 Heat and fluid flow patterns for positive eccentric annuli, $\varepsilon = 0.625$, at different Ra* and Pr

butions at various Ra* and Pr for positive and negative eccentricity, respectively. For positive eccentric geometry (Figure 3) it is evident that the convective flows are both larger and stronger than for the concentric annulus. Within such favorable configuration for convective motion, the qualitative features of heatline and isotherm distributions depicted previously for the concentric geometry are observed to be further pronounced. At high Ra*, the expanse of the heat-receiving region on the outer wall is considerably extended for the positive eccentric arrangement in contrast to the concentric annulus. On the other end, the negative eccentric geometry provides least favored circumstance for the development of natural convection. Both the size and strength of the fluid flow are markedly reduced as shown in Figure 4. The heatlines in the figure reveal that with the enlarged isothermal zone in the bottom of the negative eccentric annulus at $Ra^* \geqq 10^4$ heat from the inner wall flows primarily toward the top portion of the outer cylinder. Also, the weak effect of the Prandtl number on the heat and fluid flow patterns for the eccentric geometries considered can be readily inferred from Figures 3 and 4.

Surface temperature of inner cylinder

For the specified uniform heat flux condition on the inner cylinder, the surface temperature is one of the important variables in the present calculations, since it can reflect the local heat transfer characteristics along the inner cylinder. The circumferential temperature distribution along the inner cylinder at various Ra* and Pr are presented in Figures 5–7 for the three configurations under study. Note that in the present normalization the local Nusselt number along the inner cylinder is simply the inverse of the dimensionless surface temperature. Thus the angular variations of the local Nusselt number under various conditions can be deduced from these figures. Common to the results displayed for the three geometries is that as the modified Rayleigh number increases, the local dimensionless surface temperature of the inner cylinder decreases, indicative of a higher rate of heat transfer due to the stronger buoyancy flow in the annulus. For the concentric annulus, as expected, an isothermal surface temperature profile occurs for pure conduction, $Ra^* = 0$ as illustrated in Figure 5. The enhanced convective fluid flow in the annulus with increasing Ra* causes a significant variation of the surface temperature along the circumference of the inner cylinder at $Ra^* = 10^3$. The local surface temperature increases from the bottom to the top of the inner cylinder. As Ra* further increases, the magnitude of the circumferential variation of surface temperature is greatly diminished except in the region of thermal plume having a distinct temperature rise.

Similar observations can be made for the positive eccentric geometry considered (Figure 6). As for the negative eccentric annulus, Figure 7, the temperature profile along the inner

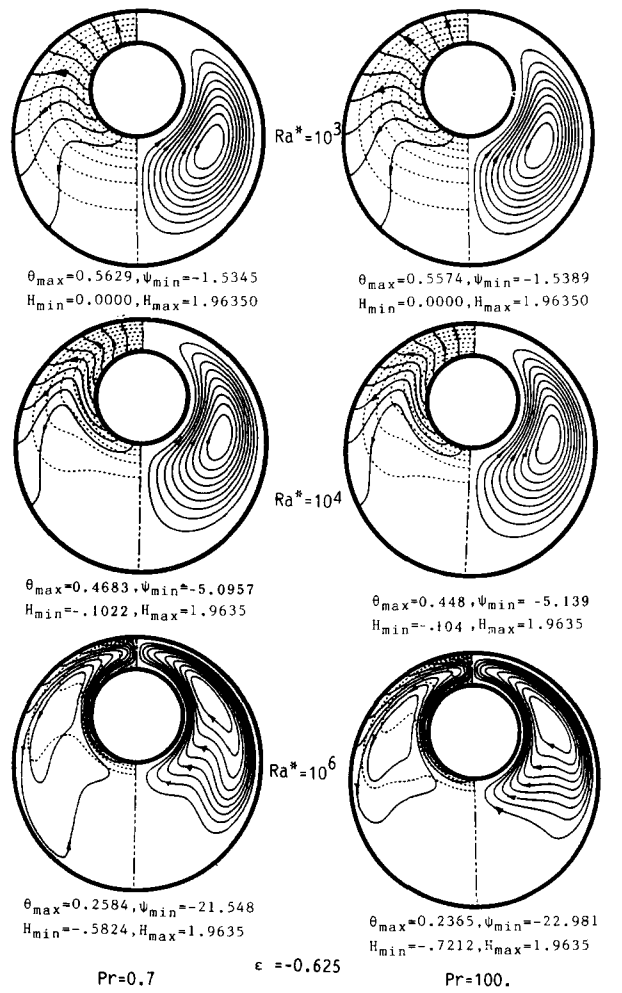

Figure 4 Heat and fluid flow patterns for negative eccentric annuli, $\varepsilon = -0.625$, at different Ra* and Pr

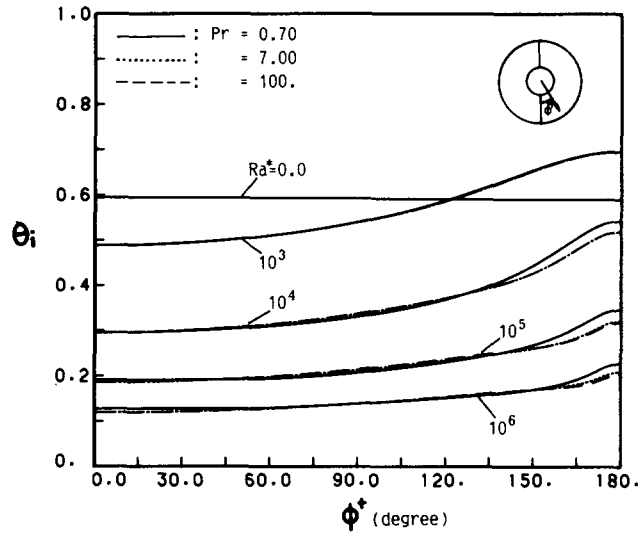

Figure 5 Local surface temperature distribution on the inner cylinder for $\varepsilon = 0.0$

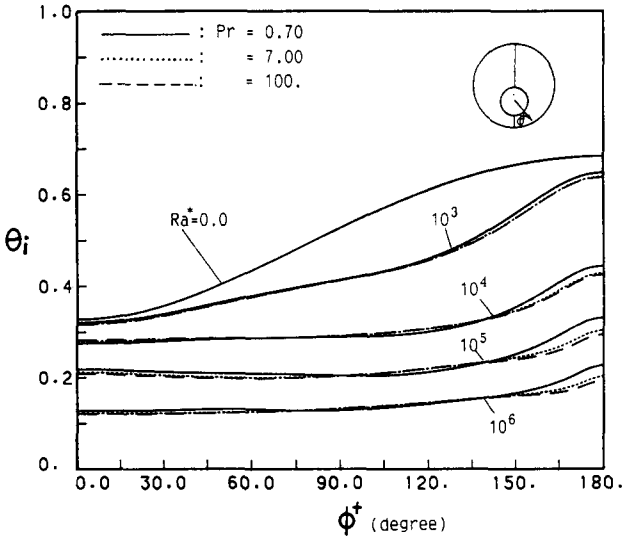

Figure 6 Local surface temperature distribution on the inner cylinder for $\varepsilon = 0.625$

cylinder for the pure conduction is opposite to that for the positive eccentric geometry shown in Figure 6. The surface temperature decreases monotonically from the bottom to the top of the cylinder. As Ra* increases, the location of the maximum surface temperature shifts gradually from the bottom toward the top of the inner cylinder. For $Ra^* \geq 10^5$, a temperature profile similar to the cases described above can be clearly detected from the figure.

Similar observations concerning the variation of surface temperature on the inner cylinder with specified heat flux have been reported in the previous study for heat flux boundary conditions.[4] Furthermore, from Figures 5–7 it can be seen that the local surface temperature profile of the inner cylinder is rather insensitive to the investigated range of variation for the Prandtl number. The magnitude of the maximum surface temperature on the inner cylinder of the uniform heat flux is also another quantity of practical interest and is listed in Table 1. For comparison, the data of the maximum surface temperature available in Ref. 6 are also included in Table 1 and appear to be in good agreement with those predicted in the present study. Moreover, the maximum surface temperature for both $\varepsilon = 0$ and 0.625 can be well correlated via a least square regression with the modified Rayleigh number and the Prandtl number as follows:

$$\varepsilon = 0: \quad \theta_{max} = 3.09332(Ra^*)^{-0.191} Pr^{-0.015} \qquad (9a)$$
$$10^4 \leq Ra \leq 10^6, \quad 0.7 \leq Pr \leq 100$$

$$\varepsilon = 0.625: \quad \theta_{max} = 2.44619(Ra^*)^{-0.173} Pr^{-0.011} \qquad (9b)$$
$$10^3 \leq Ra^* \leq 10^6, \quad 0.7 \leq Pr \leq 100$$

The maximum deviations of the above correlations from the numerical data are 3.5% and 4.5%, respectively. For the results of the negative eccentric annulus $\varepsilon = -0.625$, no satisfactory correlation was found.

Local heat flux distribution

Distribution of the local heat flux along the surface of the outer cylinder, q_o, will now be presented. In considering a dimension-

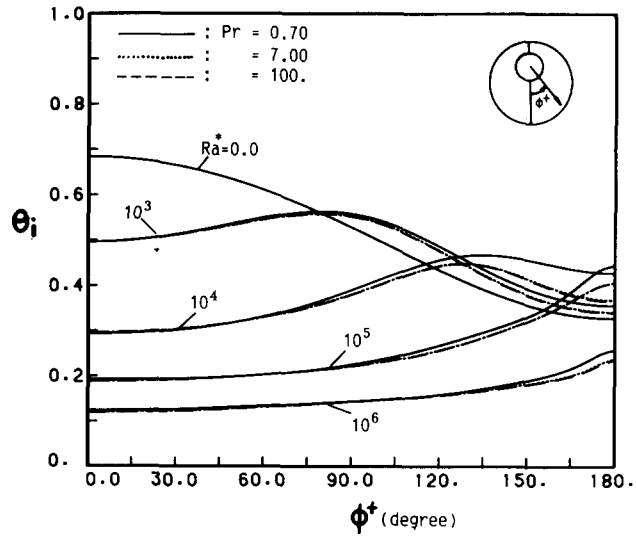

Figure 7 Local surface temperature distribution on the inner cylinder for $\varepsilon = -0.625$

Table 1 Maximum surface temperature on the inner cylinder

		θ_{max} for Ra*			
ε	Pr	10^3	10^4	10^5	10^6
0.625	0.7	0.6484	0.4447	0.3317	0.2274
	7.0	0.6393	0.4286	0.3040	0.2037
	50.0	0.6385	0.4265	0.2918	0.1972
	100.	0.6381	0.4251	0.2877	0.1948
0.000	0.7	0.6962	0.5258 (0.5055)*	0.3479 (0.3412)*	0.2294
	7.0	0.6956	0.5139	0.3221	0.2117
	50.	0.6953	0.5131	0.3204	0.2076
	100.	0.6951	0.5127	0.3199	0.2055
−0.625	0.7	0.5629	0.4684	0.4454	0.2584
	7.0	0.5579	0.4488	0.4072	p.2387
	50.	0.5576	0.4485	0.4066	0.2372
	100.	0.5574	0.4484	0.4064	0.2365

* From Ref. 6.

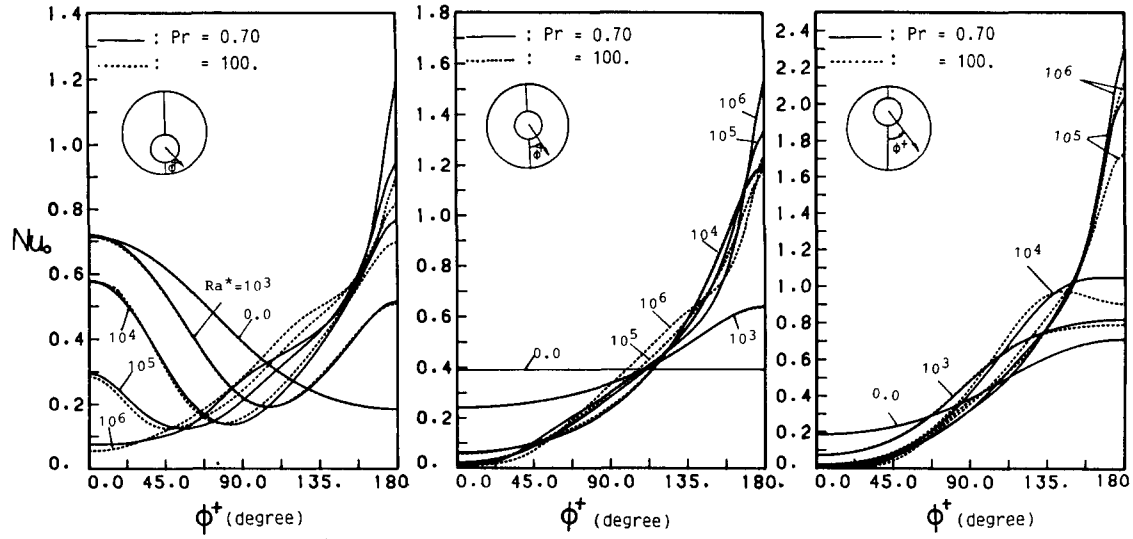

Figure 8 Local heat flux distributions on the outer cylinder

Table 2 Maximum heat flux on the outer cylinder

		$(Nu_o)_{max}$ for Ra*			
ε	Pr	10^3	10^4	10^5	10^6
0.625	0.7	0.7205	0.7651	0.9446	1.1928
	7.0	0.7173	0.7151	0.8637	1.0211
	50.0	0.7150	0.7053	0.8225	0.9494
	100.	0.7142	0.7021	0.8176	0.8977
0.000	0.7	0.6426	1.1998	1.3341	1.5994
	7.0	0.6411	1.1812	1.2394	1.3644
	50.	0.6404	1.1730	1.1940	1.2401
	100.	0.6402	1.1700	1.1882	1.2140
−0.625	0.7	0.8229	1.0502	2.0333	2.3045
	7.0	0.8066	0.9677	1.8794	2.1803
	50.	0.7985	0.9234	1.7915	2.1406
	100.	0.7943	0.9088	1.7336	2.1365

less representation of the local heat flux, a local Nusselt number is defined as

$$Nu_o=\frac{q_o}{q_i}=-\left[1+\left(\frac{1}{\pi F}\frac{\partial F}{\partial \phi}\right)^2\right]^{1/2}\frac{\partial \eta}{\partial r}\frac{\partial \theta}{\partial \eta}\bigg|_{\eta=1} \tag{10}$$

Figure 8 conveys the angular distribution of the local heat flux along the outer cylinder of the three geometries considered for two values of Pr with various Ra*. The results for the concentric and negative eccentric geometries are qualitatively rather similar and will then be discussed together. At $Ra^*=10^3$, the local heat flux increases from the bottom to the top of the outer cylinder. With increasing Ra*, the angular variation of the local heat flux becomes more pronounced such that the heat transport is highly concentrated in the upper half of the outer cylinder. The heat flux at the bottom of the outer cylinder is rather negligible. For the positive eccentric annulus, as expected for the case of pure conduction $Ra^*=0$, the heat flux decreases from the bottom to the top of the outer cylinder. With increasing Ra*, the heat flux dropoff (increase) along the bottom (upper) half of the outer cylinder exhibited in the figure manifests the intensification of the convective motion in the annulus. At $Ra^*=10^6$, a local heat flux distribution similar to those for $\varepsilon=0$ and -0.625 is observed. The foregoing nature of the local heat flux distributions can be further inferred from the heatline distributions shown in Figures 1–4.

Moreover, Figure 8 reveals that the local heat flux becomes more senstive to the variation of the Prandtl number with increasing Ra*, particularly for the peak values of the local heat flux on the outer cylinder, which are tabulated in Table 2. For all Ra*, the maximum heat flux decreases with increasing Pr; specifically, a considerable decrease of about 17% can be observed by changing Pr from 0.7 to 7.0 for the case of $\varepsilon=0.625$ at $Ra^*=10^6$. Also, the increase of the maximum heat flux with Ra* displayed in Table 2 reflects the thinning of the boundary layer along the outer cylinder. Except for $\varepsilon=-0.625$, the results of the maximum heat flux on the outer cylinder tabulated in Table 2 agree well with the following correlations:

$\varepsilon=0.625$

$$\text{Pr}=0.7,\quad (Nu_o)_{max}=0.3136(Ra^*)^{0.0964} \tag{11a}$$
$$10^4\le Ra^*\le 10^6,\quad \text{max. deviation}=0.7\%$$

$$7\le \text{Pr}\le 100,\quad (Nu_o)_{max}=0.4257(Ra^*)^{0.0651}\text{Pr}^{-0.0428} \tag{11b}$$
$$10^4\le Ra^*\le 10^6,\quad \text{max. deviation}=3.9\%$$

$\varepsilon=0.0$

$$\text{Pr}=0.7,\quad (Nu_o)_{max}=0.6668(Ra^*)^{0.0624} \tag{11c}$$
$$10^4\le Ra^*\le 10^6,\quad \text{max. deviation}=2.5\%$$

$$7\le \text{Pr}\le 100,\quad (Nu_o)_{max}=1.0776(Ra^*)^{0.0171}\text{Pr}^{-0.0217} \tag{11d}$$
$$10^4\le Ra^*\le 10^6,\quad \text{max. deviation}=4.1\%$$

Average Nusselt number

Finally, the average heat transfer results will be presented by means of the average Nusselt number, defined as

$$\overline{Nu}=\frac{q_i L}{k(\bar{T}_i-T_o)}=\frac{1}{\bar{\theta}_i} \tag{12}$$

The circumferentially averaged Nusselt numbers obtained in the present study are given in Table 3 for various Ra* and Pr in the three annular geometries under consideration. Also included in Table 3 are the results based on the correlation for the concentric geometry reported in Ref. 6, which compare favorably with the results obtained in the present study. An overview of Table 3 reveals that only a slight effect of the

Table 3 Average Nusselt number

ε	Pr	$\overline{Nu}$ for Ra* 10^3	10^4	10^5	10^6
0.625	0.7	2.2724	3.2071	4.4821	6.8942
	7.0	2.2967	3.2097	4.5226	7.1130
	50.0	2.3000	3.2129	4.5663	7.1794
	100.	2.3023	3.2142	4.5759	7.1881
0.000	0.7	1.7311 (1.6744)*	2.7638 (2.7599)*	4.4184 (4.5385)*	6.7294 (7.4167)*
	7.0	1.7329	2.7670	4.4638	6.8678
	50.	1.7334	2.7698	4.4822	6.9000
	100.	1.7338	2.27732	4.4945	6.9412
−0.625	0.7	2.0486	2.6108	3.9119	6.3904
	7.0	2.0775	2.7207	4.0300	6.5909
	50.	2.0800	2.7238	4.0412	6.6524
	100.	2.0812	2.7247	4.0500	6.6658

* From Ref. 6.

Table 4 Constants of Equation 13 for various ε

ε	C	m	n	Ra*	Max. deviation (%)
0.625	0.7276	0.1617	0.0039	10^3–10^6	4.3
0.000	0.4368	0.1997	0.0027	10^3–10^6	2.4
−0.625	0.4371	0.1936	0.0079	10^4–10^6	4.0

Prandtl number in the investigated range exists on the average Nusselt number for the three configurations considered. The average Nusselt number increases slightly with increased Prandtl number. It can then be concluded that the average heat transfer rate across the annulus is mainly dependent on the modified Rayleigh number and the eccentricity. Accordingly, the present results can be correlated via a least square regression analysis in the form

$$\overline{Nu} = C(Ra^*)^m Pr^n, \qquad 0.7 \le Pr \le 100 \tag{13}$$

where the constant C and exponents m, n are listed in Table 4 for the three configurations considered here.

In Figure 9 the average Nusselt number is plotted versus the modified Rayleigh number. For comparison, correlations reported for the similar configuration with isothermal[13] and heat flux boundary conditions[4] are also plotted in the figure. The correlations determined in Ref. 13 for isothermal boundary conditions were, however, expressed in terms of the conventional Rayleigh number Ra, not the modified Rayleigh number Ra*. Noting that $Ra^* = \overline{Nu}\,Ra$, their correlations can then be rewritten in terms of Ra* as follows:

$$\varepsilon = 0: \qquad \overline{Nu} = 0.4347(Ra^*)^{0.1955}, \quad Ra^* > 21364 \tag{14a}$$

$$\varepsilon = 0.625: \qquad \overline{Nu} = 0.5827(Ra^*)^{0.1763}, \quad Ra^* > 24165 \tag{14b}$$

$$\varepsilon = -0.625: \qquad \overline{Nu} = 0.3597(Ra^*)^{0.2089}, \quad Ra^* > 19904 \tag{14c}$$

For all three geometries considered here, the average Nusselt number for the mixed boundary conditions is larger than that for the isothermal boundaries. An analogous finding was also reported in Ref. 6 for the air-filled concentric annulus. Closer examination of Figure 9 reveals that the increase of the average Nusselt number for the mixed boundary conditions is less prominent for the negative eccentric geometry due to its least favorable circumstance for natural convention. Further, one

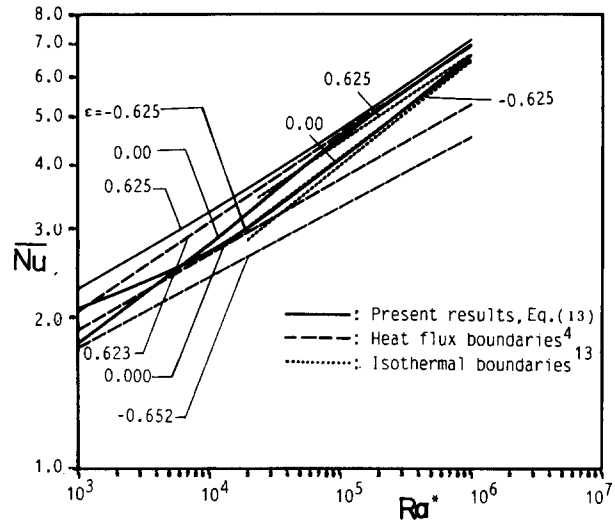

Figure 9 Variation of average Nusselt number with modified Rayleigh number

can notice that for the concentric annulus the heat flux boundaries yield the smallest average Nusselt number, providing the least favorable situation for the heat transport across the annulus among the three kinds of boundaries shown in the figure. Above all, the figure clearly demonstrates that the specification of different thermal boundary conditions has a significant influence on the average heat transfer rate across the annulus.

Concluding remarks

Natural convection in concentric and eccentric horizontal cylindrical annuli with mixed boundary conditions is analyzed numerically via a finite difference method. The heat and fluid flows in the annuli have been vividly visualized by means of contour maps of heatlines and streamlines. The numerical results obtained further indicate that heat and fluid flow patterns in the annuli are primarily dependent on the modified Rayleigh number and eccentricity and are rather insensitive to the investigated Prandtl number range. Particularly, no apparent dependence of Pr can be detected for $Pr \ge 7$. Above all, the heat transfer results show that the specification of different thermal boundary conditions has a significant influence on the average heat transfer rate across the annulus.

Acknowledgments

The authors would like to express their sincere thanks to National Cheng Kung University for providing the necessary computing facility and time. The constructive comments of the reviewers are also highly appreciated.

References

1 Kuehn, T. H. and Goldstein, R. J. An experimental and theoretical study of natural convection in the annulus between horizontal concentric cylinders. *J. Fluid Mech.*, 1976, **74**, 695–719

2 Kuehn, T. H. and Goldstein, R. J. An experimental study of natural convection heat transfer in concentric and eccentric horizontal cylindrical annuli. *ASME J. Heat Transfer*, 1978, **100**, 635–640

3 Rao, Y. F., Miki, K., Fukuda, K., and Kakata, Y. Flow pattern of natural convection in horizontal cylindrical annuli. *Int. J. Heat Mass Transfer*, 1985, **28**, 705–714

4 Glakpe, E. K., Watkins, C. B., Jr., and Cannon, J. N. Constant heat flux solutions for natural convection between concentric and eccentric horizontal cylinders. *Numerical Heat Transfer*, 1986, **10**, 279–295

5 Van de Sande, E. and Hamer, B. J. G. Steady and transient natural convection in enclosures between horizontal circular cylinders (constant heat flux). *Int. J. Heat Mass Transfer*, 1979, **22**, 361–370

6 Kumar, R. Numerical study of natural convection in a horizontal annulus with constant heat flux on the inner wall. Proc. 1987 ASME–JSME Thermal Engineering Joint Conf., Vol. 2, 187–193

7 Glakpe, E. K. and Watkins, C. B. Effect of mixed boundary conditions on natural convection in concentric and eccentric annular enclosure. AIAA paper #87-1591, the 22nd Thermophysics Conf., Honolulu, Hawaii, June 1987

8 Yao, L. S. Analysis of heat transfer in slightly eccentric annuli. *ASME J. Heat Transfer*, 1980, **102**, 270–284

9 Leonard, B. P. A convectively stable, third order accurate finite-difference method for steady two-dimensional flow and heat transfer. In *Numerical Properties and Methodologies in Heat Transfer*, ed. T. M. Shih, Hemisphere, Washington, D.C., 1983, 211–226

10 Anderson, D. A., Tannehill, J. C., and Pletcher, R. H. *Computational Fluid Mechanics and Heat Transfer*, Hemisphere, Washington, D.C., 1984

11 Schneider, G. E. and Zedan, M. A modified strongly implicit procedure for the numerical solution of field problems. *Numerical Heat Transfer*, 1981, **4**, 1–19

12 Kimura, S. and Bejan, A. The heatlines visualization of convective heat transfer. *ASME J. Heat Transfer*, 1983, **105**, 916–919

13 Projahn, U. and Beer, H. Prandtl number effects on natural convection heat transfer in concentric and eccentric horizontal cylindrical annuli. *Warme- und Stoffubertragung*, 1985, **19**, 249–255

14 Kuehn, T. H. and Goldstein, R. J. A parametric study of Prandtl number and diameter ratio effects on natural convection heat transfer in horizontal cylindrical annulus. *ASME J. Heat Transfer*, 1982, **102**, 768–770